# Transport dynamics of charged colloidal particles during directional drying of suspensions in a confined microchannel

Jize Sui*

*Center of Soft Matter Physics and its Applications, Beihang University, Beijing 100191, China*
*and School of Physics and Nuclear Energy Engineering, Beihang University, Beijing 100191, China*

(Received 25 January 2019; published 18 June 2019)

Directional drying of colloidal suspensions, experimentally observed to exhibit mechanical instabilities, is a nonequilibrium procedure that is susceptible to geometric confinement and the properties of colloidal particles. Here, we develop an advection-diffusion model to characterize the transport dynamics for unidirectional drying of a suspension consisting of charged particles in a confined Hele-Shaw cell. We consider the electrostatic interactions by means of the Poisson-Boltzmann cell approach with the viscous flow confined to the cell. By solving the nonequilibrium transport equations, we clarify how the multiple parameters, such as drying rate, confinement ratio, and the monovalent slat concentration, affect the transport dynamics of charged colloidal particles. We find that the drying front recedes into the cell with linear behavior, while the liquid-solid transition front recedes with power law behaviors. The faster evaporation rate creates a rapid formation of the drying front and produces a thinner transition layer. We show that confinement is equivalent to raising the effective concentration in the cell, and, accordingly, the drying front appears earlier and grows more rapidly. Under geometric confinement, a longer fully dried film is created while the total drying time is shortened. Moreover, we have theoretically illustrated that low salt loadings cause a large collective diffusivity of charged colloidal particles, which results in a colloidal network by aggregation. Thus, the drying behavior alters dramatically as salt loadings decrease, since the resulting compacted clusters of charged particles eventually convert the suspension into a gel-like material instead of a simple fluid. Our model is consistent with the current experiments and provides a simple insight for applications in directional solidification and microfluidics.

DOI: 10.1103/PhysRevE.99.062606

## I. INTRODUCTION

Drying behaviors occur ubiquitously in nature and daily life, most simply as the natural air-dry process, drying of a droplet and a liquid film. To understand drying phenomena, numerous multidisciplinary knowledge over spatiotemporal multiscales ranging from fluid mechanics, thermodynamics, and heat-mass transfer [1,2] should be involved. As is well known, vertical drying of colloidal or polymeric droplets and films on a flat substrate can often lead to ring-like patterns, such as coffee-ring [3,4], multiple concentric rings, even fractal-like rings [5]. These drying behaviors proceed in the absence of any geometric confinements.

Instead, horizontal drying often proceeds within a confined geometry, which can exhibit distinct characteristics from the vertical drying process. For example, horizontal drying is typically performed by sandwiching a droplet between two glass slides [6–8] or by injecting a solution to partially fill a capillary or microchannel, e.g., a micro Hele-Shaw (H-S) cell [9–11]. Horizontal drying of colloidal droplets or films has therefore generated a great deal of attention due to its practical route for directional solidification. One study of particular interest is that of cracking patterns, pioneered by Allain *et al.* [12] and later studied by Dufresne *et al.* [13,14]. Until now, the formation dynamics of array, wavy, and spiral cracks, due to the horizontal drying in the compaction zone of particles has been presented experimentally and theoretically [15–18]. Another pattern, shear bands [19], has been found in the dense deposits behind the drying front. A recently proposed mechanism by Goehring *et al.* [20] has clarified the origin of shear bands in physics: the electrostatic interplay between the charged colloidal particles and the surrounding salt solvent may play a crucial role. Besides, the order/disorder phase transition [21], as well as the phenomenon of structural anisotropy of particles [22], has also been observed in dense deposits by the horizontal drying. Recent experiments revealed that the drying rate, size of the channel, and the properties of particles (e.g., radii and aggregations) all control the formation kinetics of local cracks and the crystallinity in the dense deposits [23].

It is now clear that all these resulting patterns are formed with morphologies, which, while beautiful, often limit the utility of materials. Elaborate control of the resulting structures of the materials during directional drying performs a crucial role in materials manufacturing and other applications, such as ink-jet printing, micro- and nanocoatings, and adhesives, and biochemical deposition of DNA and RNA microarrays [24]. To explore the problems related to these applications, it is necessary to clearly understand the transport dynamics of charged colloidal particles by unidirectional drying in a confined microchannel. The existing kinetic models to scale fracture formation and concentration in directional solidification have been either proposed empirically by fitting experiments [13,14] or conducted employing simple linear

*suijize2008@126.com

 

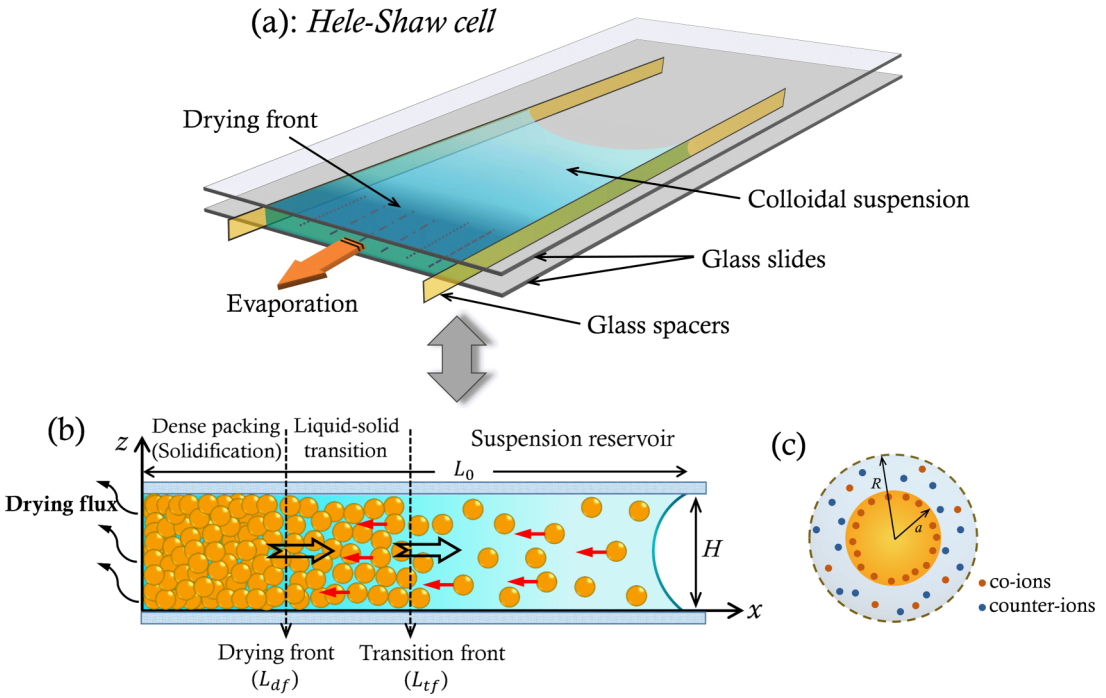


FIG. 1. (a) The schematic illustration of the directional drying of suspensions with the dispersed charged colloidal particles in a confined Hele-Shaw cell. (b) The sketch of transport dynamics of the charged particles through a cross section of the cell, which is directly used for our 1D configuration model. In the liquid-solid transition front, particles collide with each other, hindering transport. The drying front (solidification) and the liquid-solid transition front recede together towards the interior cell (indicated by black arrows), while the particles are carried towards the drying end (indicated by red arrows). (c) The Poisson-Boltzmann cell model, an electrically neutral cell is conceived to surround an individual charged particle influenced by the interplay between the ions at the surface and in the ambient solution.

approximations [9,10]. Two decades ago, Routh and Russel developed the one-dimensional (1D) kinetic model to describe the horizontal drying front of dried latex films on a flat substrate [25]. As an extension of Russel's work, an advection-diffusion model taking the hydrostatic pressure and the collective diffusion of particles into account was given recently [18]. Nevertheless, these theoretical models still missed the geometric confinement of the microchannel and the electrostatic interplay among charged colloidal particles in high concentration. A recent work has shown that the interplay between the charged particles and the surrounding ions in the solution exerts significant influence on the collective diffusivity of dispersed particles in the suspensions that are unidirectionally dried in a confined microcell [26–28]. Still poorly explored is how these factors determine the distinctive solidification dynamics during the directional drying of colloidal suspensions.

In this paper, we develop a simple kinetic model with a 1D configuration to represent the transport dynamics of charged colloidal particles in directional drying of suspensions in a confined microchannel. Experimentally, observations of the drying processes in confined geometry, for instance, a droplet between two circular glass slides [8] and a colloidal film in a H-S cell with altered size [11], have been achieved, but the relevant studies using dynamic theory have not been discussed in depth. Moreover, to characterize the interactions among the charged particles, we follow the approach of the Poisson-Boltzmann cell (PBC) model [28–31]. Figure 1(a) displays the investigated process of directional drying in a confined H-S cell. Figure 1(b) shows the sketch of the drying front and the liquid-solid transition front, both of which have been observed in the experiments. Figure 1(c) shows the structure of an individual charged particle based on the PBC model. We will derive the nonequilibrium advection-diffusion model incorporating multifactors above and clarify their resultants on the transport dynamics in directional drying.

## II. THEORETICAL FRAMEWORK

We consider a water-based suspension with dispersed charged colloidal particles unidirectionally dried in a H-S cell with height $H$. The H-S cell has two open ends. The left end is the drying end, and the right end contains a liquid-air interface [see Figs. 1(a) and 1(b)]. The suspension was injected from the left side towards the H-S cell to form a thin film with initial length $L_0$. In our model, we set a Cartesian coordinate system at the drying end and designate the $x$-axis direction as positive. The suspension therefore flows as a bulk against the $x$-axis direction due to evaporation. Only water can be dried out of the cell, thus the average volume flux of water per unit area and time can determine a drying process. In other words, the measured average velocity of evaporative water $\vec{v}_f$ can function as a proxy for the average evaporation rate of a drying system [2,10]. It is reported that the flow of water could be uniform through the microcell, even in the wet solid-like porous section at the drying end [2,10,11,13]. This observation allows us to assume uniform evaporation at a constant average rate $\vec{v}_f$. As the drying proceeds, loss

of water by evaporation is replenished by water from the reservoir, which creates a flow of bulk suspension carrying particles towards the drying end. Thus, we can naturally define the suspension (or medium) velocity as the volume average velocity

$$\vec{v}_s = \phi\vec{v}_p + (1-\phi)\vec{v}_f, \tag{1}$$

where $\vec{v}_p$ is the velocity of colloidal particles, and $\phi$ is the volume fraction of particles. Equation (1) also indicates that the suspension velocity is somewhat close to the water velocity before dense packing solidification is reached. (In reality, the medium velocity is the same as the solvent velocity in the absence of particles).

Initially, the particles in the reservoir are forced to travel together with the suspension at the average evaporation rate $\vec{v}_f$. As time goes on, the colloidal particles will slow down to accumulate at the drying end where $\vec{v}_p = 0$, while the bulk suspension can still flow at the drying end with the velocity $\vec{v}_s = (1-\phi)\vec{v}_f$ due to evaporative water. The bulk flow of suspension can carry more particles towards the drying end. Finally, a fully dried film is left when water is completely dried. During such a process, the mass of particles satisfies the conservation law

$$\dot{\phi} = -\frac{\partial\phi\vec{v}_p}{\partial x} = \frac{\partial}{\partial x}((1-\phi)\vec{v}_f - \vec{v}_s). \tag{2}$$

The suspension velocity plays an intermediate role in determining the time evolution of particle concentration. Here, the gravitational effect (e.g., the sedimentation instability) can be negligible due to the geometric confinement of a H-S cell. We can take the flow of suspension in such a confined cell to be a low Reynolds number flow. Herein, the Stokes flow equation is employed by ignoring the inertial term

$$\eta(\phi)\frac{\partial^2\vec{v}_s}{\partial z^2} = \frac{dp}{dx} + \frac{\partial\Pi}{\partial x}, \tag{3}$$

where $\eta(\phi)$ is the viscosity of the suspension that is usually susceptible to particle concentration. Equation (3) shows that the viscous dissipation of flow is balanced by the gradients of osmotic pressure arising from the evaporative water. The first item on the right side of Eq. (3) is the capillary pressure gradient that pulls water through the solid-like porous deposits to replenish loss of water by evaporation. The second item is the osmotic pressure gradient from the charged colloidal particles. Here, we assume that the flow configuration is fully developed, then the variables on the right side of Eq. (3) are only the functions of $x$. Using the no-slip boundary condition $\vec{v}_s(z=0) = \vec{v}_s(z=H) = 0$, we can obtain the suspension velocity as

$$\vec{v}_s = \frac{1}{2\eta(\phi)}\left(\frac{dp}{dx} + \frac{\partial\Pi}{\partial x}\right)(z^2 - Hz). \tag{4}$$

In practice, the velocity profile of fluid with such quadratic form is not always the case when the fluid in the reservoir flows through the dense packing zone along the $x$ and $z$ axes, which may be a complicated 2D (even 3D) problem. But here, we will focus on the average velocity over a cross section of the cell along the $x$-axis direction only, and then simplify the present problem into a 1D configuration. Such an average velocity of the suspension is therefore given by

$$\vec{v}_s = -\frac{H^2}{12\eta(\phi)}\left(\frac{dp}{dx} + \frac{\partial\Pi}{\partial x}\right). \tag{5}$$

Among the numerous models of apparent viscosity of particulate suspension proposed as a function of concentration, the Krieger-Dougherty correlation is perhaps most commonly used [2,32]

$$\eta(\phi) = \eta_0\left(1 - \frac{\phi}{\phi_m}\right)^{-\alpha\phi_m}, \tag{6}$$

where $\eta_0$ is the viscosity of water (or solvent), $\phi_m$ is the maximum volume fraction of particles at which the flow can occur without gelation, and the constant is set as $\alpha = 2.5$ following Einstein's theory for hard spherical particles. The capillary pressure gradient exists to drag water through the porous deposits of particles, which can be expressed by Darcy's law [13,15,16,28,33]

$$\frac{dp}{dx} = -\frac{\eta_0}{\kappa(\phi)}(1-\phi)(\vec{v}_f - \vec{v}_p), \tag{7}$$

where the viscosity is assumed to be that of interstitial water in the deposits zone, and the permeability $\kappa(\phi)$ is determined by the empirical formula reported by Russel *et al.* [33,34] for the suspensions of hard sphere with radius $a$

$$\kappa(\phi) = \frac{2a^2}{9\phi}(1-\phi)^6. \tag{8}$$

For the suspensions of the charged particles, the total osmotic pressure is assumed to be the expression

$$\Pi(\phi) = \frac{k_BT}{\sigma}\phi(f_s + f_q), \tag{9}$$

where $\sigma$ is the volume of an individual charged particle, and $k_BT$ is the thermal energy. As Eq. (9) shows, the entropic item $f_s$ and the electrostatic item $f_q$ both contribute to the osmotic pressure of the suspensions. Many approximate models of the compressibility factor $f_s$ have been suggested by taking the interparticle interactions at high concentration, such as the Carnahan-Starling equation (valid for $0 \leqslant \phi \leqslant 0.55$) [33]. In this work, we will model $f_s$ by introducing a divergence concentration $\phi_c$, because a certain packing concentration is often observed in the dense solid deposits behind the drying front [10,23,33]. An empirical expression of $f_s$ that is valid over the entire range of concentration is given by [33]

$$f_s(\phi) = \frac{1 + a_1\phi + a_2\phi^2 + a_3\phi^3}{1 - \phi/\phi_c}, \tag{10}$$

where the weights are given by $a_1 = 4 - 1/\phi_c$, $a_2 = 10 - 4/\phi_c$, $a_3 = 18 - 10/\phi_c$. The divergence concentration defined as the packing fraction $\phi_c$ should be measured experimentally depending on the drying conditions and the materials. As reported previously [23,33–35], the liquid crystalline phase of hard spheres will form as the concentration increases from 0.494 to 0.74, and the glass transition may occur with the concentration from 0.58 to 0.64. These concentrations for the phase transition are known as randomly close packing. Here, for the sake of simplicity, we assume randomly close packing

of $\phi_c = 0.64$ as the divergence concentration [23,33–35]. On the other hand, we would also anticipate a flowing suspension until the particle concentration reaches $\phi_c$, in other words, $\phi_m = \phi_c$ is assumed.

To examine the electrostatic contribution to the osmotic pressure, we employ the PBC model [28–31], which is assigned to quantify interactions among charged colloidal particles, such as colloidal polystyrene, silica, and nanoparticles. As the PBC model states, an electrically neutral spherical cell with radius $R$ is designated for each individual particle. The total volume of these created cells should be equivalent to the entire volume of suspension, namely $R = a/\phi^{1/3}$. The PBC model describes a deformable cloud of ions around each charged particle with radius $R$ able to shrink and expand with an increasing and the decreasing particle concentration, respectively. Here, we present a simplified version of PBE as applicable to a monovalent electrolyte with equilibrium salt concentration $n_0$, which avoids the necessity of solving the full PBE

$$\nabla^2\varphi = \kappa^2 \sinh\varphi, \tag{11}$$

where $\varphi = e\psi/k_BT$ is the reduced electrostatic potential of $\psi$, $\kappa^{-1}$ is the Debye length, and $e$ is the fundamental charge. Equation (11) can be solved within a spherical coordinate system only along radial direction $r$. The boundary conditions are that the electrostatic potential decays to 0 at the cell surface due to charge neutrality, i.e., $\partial\varphi/\partial r = 0$ at $r = R$, and the surface of particle is charged with the density $\gamma$, so $\partial\varphi/\partial r = -4\pi\gamma L_B$ at $r = a$, where the Bjerrum length is given by $L_B = \kappa^2/8\pi n_0$ ($L_B \approx 0.7$ nm in water at room temperature). The distributions of positive (+) and negative (−) ions in the cell can be determined by $n_\pm = n_0 e^{\mp\varphi}$.

At equilibrium, the osmotic pressure is the difference between the potential of ions inside the cell and those in the solution with the salt concentration $n_0$. Note that, the time scale to reach the equilibrium pressure in a cell is very short, generally on the order of 1 $\mu$s, compared to the drying time (several minutes or hours), which guarantees an equilibrium osmotic pressure during the drying procedure. We also assume the cases of the symmetric electrolyte and low surface potential. These considerations therefore give the following compressibility factor $f_q$ by

$$\begin{aligned} f_q &= \frac{4}{3}\pi R^3(n_+(R) - n_0 + n_-(R) - n_0) \\ &= \frac{\sigma}{\phi} n_0(2\cosh\varphi(R) - 2). \end{aligned} \tag{12}$$

Together with above set of equations, by introducing the expressions of velocities $v_e = -\vec{v}_e$, $v_f = -\vec{v}_f$, and $v_p = -\vec{v}_p$, the suspension velocity in Eq. (5) is then calculated as

$$v_s = \frac{1}{M(1-\phi)^5 + \chi}\left(\chi v_f + \frac{H^2(1-\phi)^5}{12\eta_0}\frac{\partial\Pi}{\partial x}\right), \tag{13}$$

where $\chi = 3\varepsilon^2/8$ with $\varepsilon = H/a$ being the confinement parameter, and $M = (1-\phi/\phi_c)^{-\alpha\phi_c}$. Incorporating Eq. (13) into the conservation law Eq. (2), we obtain the time evolution equation of the concentration as

$$\begin{aligned} \dot{\phi} = v_f\frac{\partial}{\partial x}\left(\phi + \frac{\chi}{M(1-\phi)^5 + \chi}\right) \\ + \frac{H^2}{12\eta_0}\frac{\partial}{\partial x}\left(\frac{(1-\phi)^5}{M(1-\phi)^5 + \chi}\frac{\partial\Pi}{\partial x}\right). \end{aligned} \tag{14}$$

We also assume that the suspension in the H-S cell is initially homogenous with initial particles concentration $\phi_0$. The corresponding boundary conditions are given by

$$v_s|_{x=0} = (1-\phi)v_f, \quad \left.\frac{\partial\phi}{\partial x}\right|_{x=L(t)} = 0. \tag{15}$$

Equations (14) and (15) determine the time evolution of the drying system studied here.

By invoking an additional transformation procedure, the equations mentioned above can be written into their dimensionless forms, which would be convenient for computations and discussions. Considering the liquid-air interface moving towards the drying end, the following dimensionless variables are assigned as

$$\tilde{x} = \frac{x}{L_0(1-\tau)}, \quad \tau = \frac{t v_f}{L_0}, \quad \tilde{v}_s = \frac{v_s}{v_f}. \tag{16}$$

Consequently, equations (13) and (14) are then rewritten as Eqs. (17) and (18), respectively

$$\tilde{v}_s = \frac{1}{M(1-\phi)^5 + \chi}\left(\chi + \frac{\chi(1-\phi)^5}{\mathrm{Pe}(1-\tau)}\frac{\partial\tilde{\Pi}}{\partial\phi}\frac{\partial\phi}{\partial\tilde{x}}\right), \tag{17}$$

$$\begin{aligned} \frac{\partial\phi}{\partial\tau} = \frac{1-\tilde{x}}{1-\tau}\frac{\partial\phi}{\partial\tilde{x}} + \frac{\chi}{1-\tau}\frac{\partial}{\partial\tilde{x}}\left(\frac{1}{M(1-\phi)^5 + \chi}\right) \\ + \frac{1}{\mathrm{Pe}(1-\tau)^2}\frac{\partial}{\partial\tilde{x}}\left(\frac{\chi(1-\phi)^5}{M(1-\phi)^5 + \chi}\frac{\partial\tilde{\Pi}}{\partial\phi}\frac{\partial\phi}{\partial\tilde{x}}\right), \end{aligned} \tag{18}$$

where the drying Peclet number is defined as $\mathrm{Pe} = L_0 v_f/D_0$ with $D_0 = k_BT/6\pi\eta_0 a$ being the self-diffusion constant of an individual particle, and the dimensionless osmotic pressure is given by $\tilde{\Pi} = \Pi\sigma/k_BT = \phi(f_s + f_q)$. The original moving boundary conditions are now converted to the fixed conditions

$$\tilde{v}_s|_{\tilde{x}=0} = 1 - \phi, \quad \left.\frac{\partial\phi}{\partial\tilde{x}}\right|_{\tilde{x}=1} = 0. \tag{19}$$

From Eq. (18), we can highlight the collective diffusivity as a function of particles concentration in dimensionless form

$$\tilde{D}(\phi) = \frac{\chi(1-\phi)^5}{M(1-\phi)^5 + \chi}\frac{\partial\tilde{\Pi}}{\partial\phi}. \tag{20}$$

The currently used approach of incorporating the PBC model in the collective diffusivity of charged particles is somewhat consistent with the recent work by Goehring *et al.* [28]. The dynamics part of unidirectional solidification in their work, however, has still not been explicitly discussed, as well as the confinement effects, since the model was greatly simplified to seek only the steady-state solutions. Even so, their work still exemplified the valuable experimental investigations of directional drying, which in turn benefits the theoretical studies. The charged colloidal particles in our problem are taken to be the same materials considered in

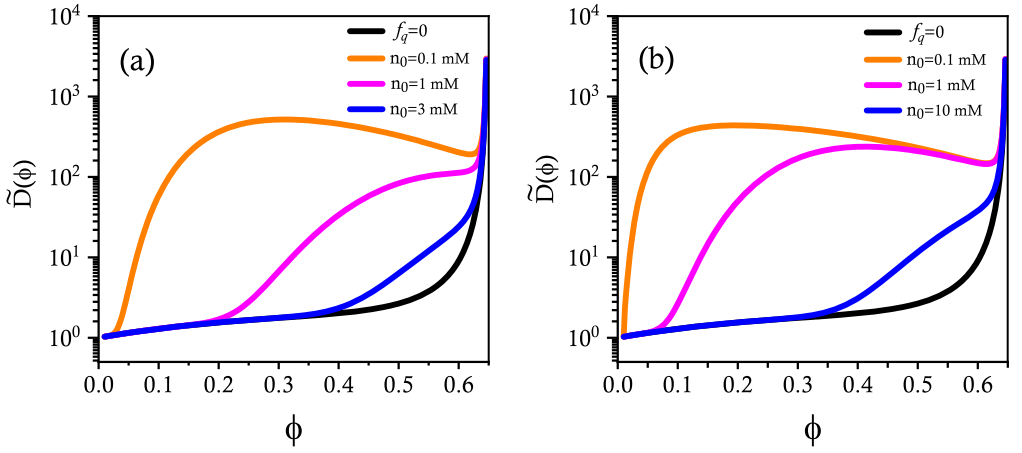


FIG. 2. The effective diffusion coefficient quantified by Eq. (20) for different colloidal particles: (a) $a = 100$ nm and $\gamma = 0.033\,\mathrm{e\,nm^{-2}}$; (b) $a = 50$ nm and $\gamma = 0.132\,\mathrm{e\,nm^{-2}}$. The black line signifies the diffusivity of uncharged particles ($f_q = 0$). The confinement parameter is $\varepsilon = 100$ for both of the cases.

the experiments of Goehring *et al.* [28], and we assume that a silica sphere with the radius $a = 100$ nm has the surface charge density $\gamma = 0.033\,\mathrm{e\,nm^{-2}}$, assuming the total surface charge is fixed. Figures 2(a) and 2(b) display that the effective diffusion coefficient varies as a function of particle concentration for the large particle $a = 100$ nm and the small one $a = 50$ nm. The effective diffusivity of charged particles is typically larger than that of uncharged ones. As the salt concentration decreases, the effective diffusivity is prominently enhanced, particularly for small charged colloidal particles, which may result in the occurrence of aggregate phenomenon in the suspensions. Experimentally, adding the certain surfactants in the suspensions is an effective approach to keeping the charged particles well dispersed [2,5].

## III. RESULTS AND DISCUSSION

In this section, we show how the directional drying is affected by multiple factors, such as evaporation rate, confinement parameter, and concentration of monovalent salt in the solution. As is well known, the evaporation rate is one of the key determinants affecting the drying process and the deposit patterns [2,5]. Evaporation is generally related to ambient temperature and saturated humidity in the vapor phase. In the present model, the evaporation rate can be quantified by the dimensionless parameter of the drying Peclet number Pe. Figure 3 shows the transport dynamics of the charged particles during the drying of suspension in the H-S cell for various Pe. For these calculations, we consider the colloidal particle with radius $a = 100$ nm and ignore the confinement effect by taking $\varepsilon = 100$. As seen in Fig. 3, the bulk flow of suspension created by the evaporative water carries the particles to accumulate at the drying end. In other words, the concentration at the drying end increases gradually until reaching the dense packing concentration. Meanwhile, the liquid-air interface far from the drying end is seen to shrink towards the drying side due to the loss of water by evaporation, but the suspension in the reservoir retains the initial concentration value $\phi_0 = 0.1$.

As illustrated in Fig. 3, an increasing evaporation rate Pe will enable particles to pile up faster against the drying end so that the dense packing zone ($\phi_c \cong 0.64$) is formed more readily. The particle velocity shown in the insets of Figs. 3(b) and 3(c) can also represent the transport behavior in which the

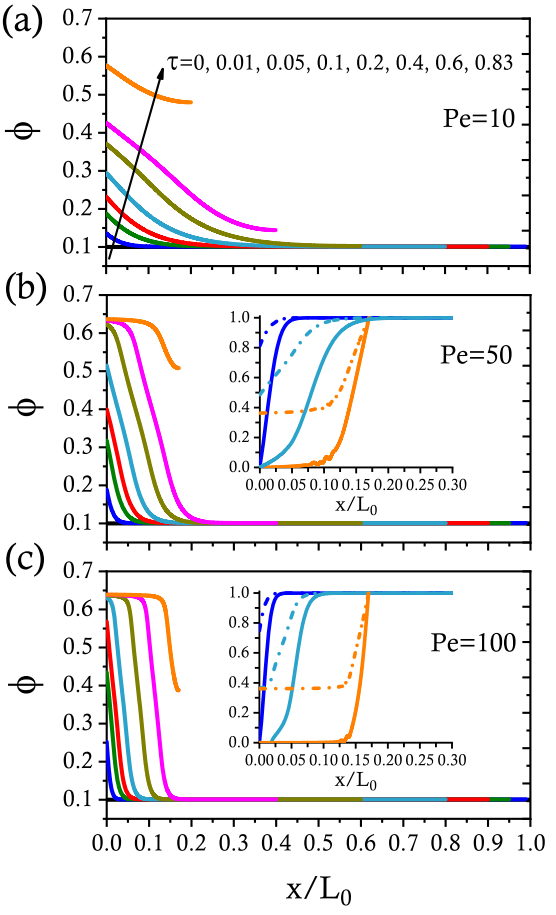


FIG. 3. The transport dynamics of the charged particles for different Peclet numbers with $\varepsilon = 100$ ignoring the confinement. The solid lines in the insets presents particle velocity $v_p$, and the dashed lines are for suspension velocity $v_s$. The parameters used for calculations are $a = 100$ nm, $\gamma = 0.033\,\mathrm{e\,nm^{-2}}$, $n_0 = 1$ mM, and $\phi_0 = 0.1$.

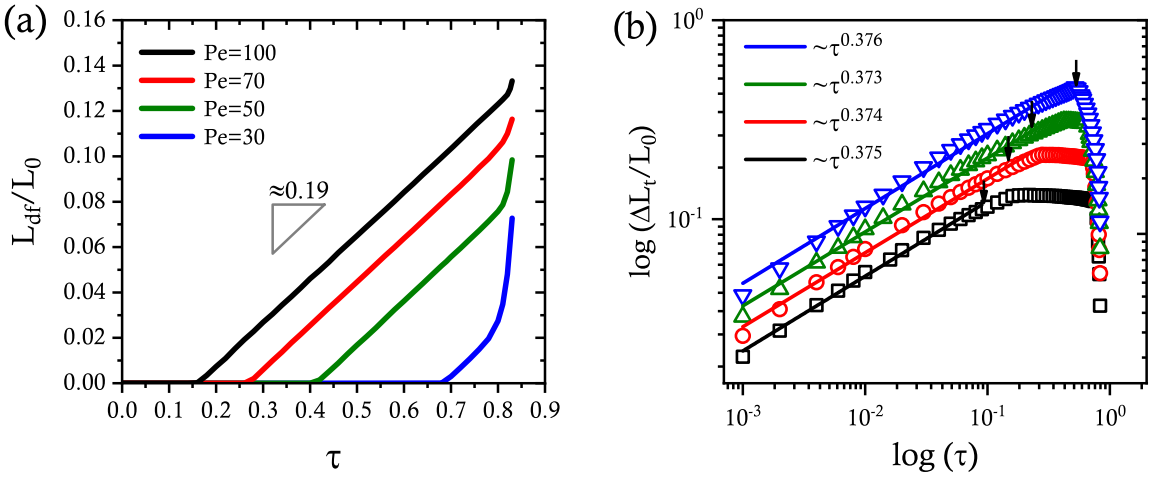


FIG. 4. (a) The time evolution of drying front and (b) liquid-solid transition layer in the log-log plot for different Peclet numbers. Other parameters used here are the same as those in Fig. 3.

particles travel initially with the suspension at the velocity $v_f$ in the reservoir but their velocities are divergent at a certain place. In other words, the particles will slow down to be kept in the dense deposits zone $v_p = 0$, while the bulk suspension is still flowing due to the continuous evaporation of water. Insets in Figs. 3(b) and 3(c) show that both the velocities of particles and suspension have a value smaller than 1, which is in accord with the previous discussions that a steady flow of water by evaporation creates the bulk flow of suspension. As the particles are compacting into their own dense deposits, the suspension flow then slows due to the relationship in Eq. (1).

As assumed earlier, the dense packing deposits will form when the particle concentration approximates to $\phi_c \cong 0.64$, which gives the appearance of drying front $L_{df}$. Obviously, the dense packing zone forms more readily with the increase of drying rate. A state called the liquid-solid transition (LST), however, can appear before the formation of the drying front [see Fig. 1(b)]. In such a state, the colloidal particles first start to pack more closely hindering their transport, which leads directly to a notable increase in concentration from the initial value. Hence, one can define the LST front $L_{tf}$ as the position in which the particle velocity starts to decrease from 1 [see Figs. 3(b) and 3(c)]. Since both of the fronts recede into the H-S cell, a transition layer $\Delta L_t = L_{tf} - L_{df}$ naturally exists between the drying front and the LST front, which also moves backward over time. This phenomenon has been observed frequently in the drying of the drops or films [15,16,28]. Note that, the appearance of drying front $L_{df}$ indicates a formation of solidification in which the suspension turns into a wet dense solid, while the concentrated suspension in the transition layer is still a liquid-like dispersion. Figure 4 shows the time evolution of the drying front and the transition layer for different evaporation rates. In Fig. 4(a), the time for a drying front becomes shorter with increasing Pe, i.e., the solidification phase appears earlier. One can find that the drying front increases linearly with time at the intermediate stage of drying. The velocity of the drying front $\tilde{v}_{df}$ scaled by the drying rate and the slope of the $L_{df}$ profile, does not change with Pe. The numerical calculations show the slope as $0.19 \pm 1.3 \times 10^{-3}$.

This linear behavior could be interpreted by means of a simple analysis with the assumption that ignoring the variation of concentration in the thin layer of the liquid-solid transition should not significantly affect the particle conservation. This assumption is generally valid, in particular for the high drying rate with a very thin LST layer. Accordingly, the conservation law of the particles can be given by

$$L_{df}\phi_c + (L - L_{df})\phi_0 = L'_{df}\phi_c + (L - \Delta t\, v_f - L'_{df})\phi_0, \tag{21}$$

where $L'_{df}$ is the position of the drying front after a time step $\Delta t$, and $L$ is the moving liquid-air interface far from the drying end. To transform Eq. (21), one can obtain the formula immediately as

$$(L'_{df} - L_{df})(\phi_c - \phi_0) = \Delta t\, v_f \phi_0. \tag{22}$$

If the time step $\Delta t$ is small enough, the difference of front $\Delta L_{df} = L'_{df} - L_{df}$ is a minimum quantity, then the velocity of the drying front is derived by

$$\tilde{v}_{df} = \frac{\phi_0}{\phi_c - \phi_0}. \tag{23}$$

Hence, Eq. (23) indicates that the velocity of the drying front is independent of Pe, and it gives an analysis value $\tilde{v}_{df} = 0.185$ for initial concentration $\phi_0 = 0.1$. Obviously, the analysis result is consistent with the numerical calculation in Fig. 4(a). This argument may be invalid for small drying rates, as the linear part of the time-dependent drying front for Pe = 30, for instance, seems to vanish.

Figure 4(b) illustrates the time evolution of the transition layer for different Pe values. Since the drying front does not appear initially [the part before the arrows in Fig. 4(b)], the transition layer is actually the growth of the LST front $L_{tf}$ over time. The growth of the LST front can be described by a power law $L_{tf}/L_0 = \alpha\tau^k$ since the log-log plots can be well fitted linearly. Based on the log-log plots in Fig. 4(b), the power index is a constant $k = 0.37 \pm 0.007$, and the prefactor $\alpha$(Pe) is the only parameter dependent upon Pe, which determines the velocity of the LST front. A similar law has been applied for the trajectories of the compaction front [13,14]. As time goes on, the drying front appears, then the transition layer $\Delta L_t$

begins to evolve back to the cell. It can be seen in Fig. 4(b) that the $\Delta L_t$ first keeps the constant value and then declines rapidly at the final stage of the drying. The higher evaporation rate gives the thinner liquid-solid transition layer, since the particles are directly compacted into the dense deposit zone by rapid evaporation of water instead of gradually undergoing the liquid-solid transition state. As the drying front recedes with the LST front, the liquid-air interface moves towards the drying end, and as a consequence, the directional drying is considered to be completed when these fronts and interfaces combine together. Importantly, during the last moment of the drying, the drying front $L_{df}$ in Fig. 4(a), as well as the layer $\Delta L_t$ in Fig. 4(b), recedes dramatically faster. The phenomenon of rapid combination of moving fronts has been referred to as the "*rush hour*" when the drying of a droplet or a film proceeds to its last moment [7,21].

As the height $H$ of the H-S cell decreases, the geometric confinement effect is going to be prominent. In this work, we consider the height constraint as only a confinement effect for approximation by assuming a large lateral size. The confinement effect is assigned the limited parameter by $\varepsilon = 6$. Besides, we also need to consider a complementary correction in the concentration due to the geometric confinement arising from the excluded volume effect near the walls. A similar consideration has been applied for the sedimentation in a narrow tube [36]. Here, with the square cross-section geometry in the H-S cell, an effective height for the confined particles becomes $H - 2a$, since the center of the particle is unable to penetrate the walls. This gives rise to an effective volume fraction higher than that in the bulk by

$$\phi_{\text{eff}} = \frac{\phi}{1 - 2/\varepsilon}. \tag{24}$$

The effective volume fraction becomes more important as $\varepsilon$ decreases. By considering Eq. (24) in the calculations, Fig. 5 manifests the time evolution of the concentration profiles for different confinement parameters. In these calculations, a Peclet number of $\text{Pe} = 50$ is used, and the particles with radius $a = 100$ nm are assumed to disperse well in the suspension with the salt loading $n_0 = 1$ mM. In Fig. 5, the initial concentration is $\phi_0 = 0.1$, but the effective initial concentration $\phi_{\text{eff0}}$ is larger than $\phi_0$ due to decreasing $\varepsilon$. With the enhanced confinement, the concentration profile at the drying end increases rapidly over time, and the time for a fully dried film is shortened, which suggests the earlier emergence of the dense packing zone. Such results agree with the experimental observations that confinements result in an enhanced directional drying process [11].

It is found that an increasing confinement effect conducts a longer solidification zone, as well as a longer completely dried film, as shown in Fig. 5. To understand this phenomenon, the velocities of the particles and the suspension are presented in Fig. 6 for time $\tau = 0.2$. The results suggest that the enhanced confinement (decreasing $\varepsilon$) noticeably diminishes the velocity of particles, especially that of particles in the reservoir. We conjecture that such decline of particle velocity in large magnitude may originate from the decrease of suspension velocity under confinement. Since the particle velocity appears as function of concentration, according to Eq. (1) $\tilde{v}_p = (\tilde{v}_s - 1 + \phi)/\phi$, once the suspension velocity is given.

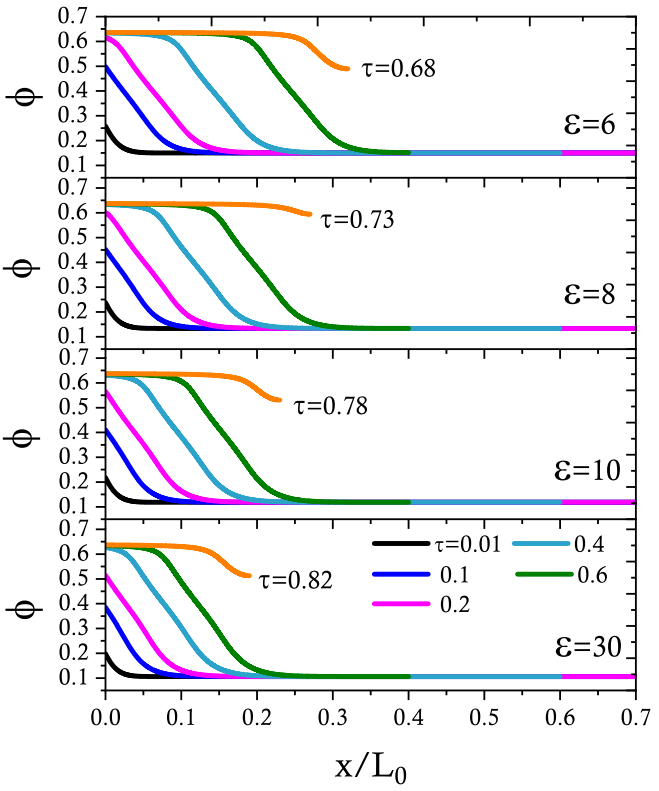


FIG. 5. The transport dynamics of the charged particles for various confinement effects at the moderate Peclet number $\text{Pe} = 50$. The other parameters are used by $a = 100$ nm, $\gamma = 0.033$ e nm$^{-2}$, $n_0 = 1$ mM, and $\phi_0 = 0.1$. The orange lines present the concentrations when a dried solid film is achieved.

The insets in Fig. 6 show that a small decline of $\tilde{v}_s$ from 0.9993 to 0.9520 with the increasing confinement (calculated for $\phi_0 = 0.1$) leads to a large drop of $\tilde{v}_p$ with concentration. These results identify that the confinement enables an increasing local concentration by slowing down the transport of colloidal particles, which also indicates why the solidification zone becomes longer for drying under confinement in Fig. 5. Moreover, the present calculations may suggest a threshold confinement characterized by $\varepsilon = 30$, above which particle transport is unaffected by the confinement, while below which the transport is notably suppressed. Note that, when the geometric confinement becomes stronger, the wetting meniscus of the liquid-air interface may also play a role in trapping the particles near the walls [8], involving the resultants of local surface tension, wall friction, and drying rate. These complex factors will not be incorporated in the present work, but they should be well addressed for the further study of the drying behaviors in a confined geometry system.

Figure 7 represents the evolution of the drying front and the transition layer $\Delta L_t$ for different confinements. Figure 7(a) shows that the drying front appears earlier and recedes backwards at a higher rate under confinement, which is consistent with our previous discussions. That is to say, the geometric confinement appears to be an important approach to achieving the enhanced drying flux and the fast solidification in a directional drying [11]. In addition, the linear behavior of the drying front can remain well only for the weak confinement

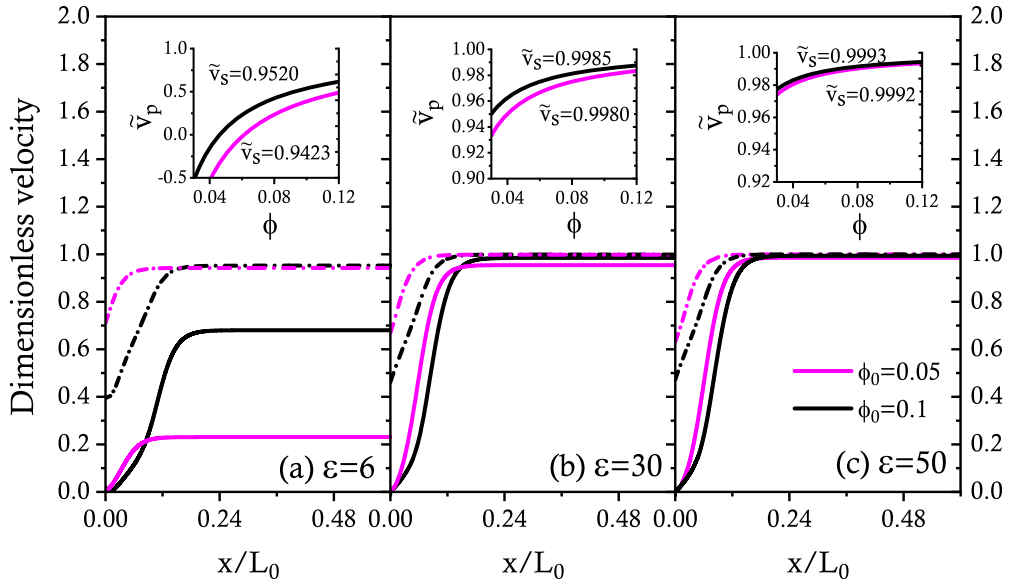


FIG. 6. The velocity of the particles (dashed lines) and the suspension (solid lines) at time $\tau = 0.2$ for various confinement parameters $\varepsilon$. The insets present that the particle velocity $\tilde{v}_p$ varies as a function of concentration $\phi$ with the given suspension velocity $\tilde{v}_s$ for different $\varepsilon$. The given $\tilde{v}_s$ in the insets are calculated by the initial concentration $\phi_0 = 0.05$ (pink) and $\phi_0 = 0.1$ (black), respectively.

$\varepsilon = 30$, otherwise the drying front increases nonlinearly over time as the confinement enhances. Figure 7(b) illustrates that the confinement not only shortens the total drying time, but also gives rise to a thinner transition layer $\Delta L_t$ during the drying process. The growth of the LST front is unaffected by the confinement, since the log-log plots suggest the same linear law, $\Delta L_t/L_0 \approx 10^{-0.32}\tau^{0.364}$, in fitting the growth profile of the LST front for different $\varepsilon$. We conclude that both the high drying rate and the confinement, combining Figs. 7 and 4, cannot only conduct a thinner liquid-solid transition layer, but also hasten the directional solidification and shorten the total drying time.

Since the colloidal particles are surface-charged, their transport behaviors could be associated with the interactions between the ions at the particle surface and those in the ambient salt solution. The electrostatic interplay, as discussed earlier, is qualified by $f_q$ in our model Eq. (12), which is related to the properties of the particles, such as the radius and the surface charge density, and also to the salt concentration $n_0$. Quantitative evidence in Fig. 2 indicates that the collective diffusivity of charged particles increases substantially as the salt concentration decreases, and this behavior of $\tilde{D}(\phi)$ is also conspicuous for the smaller particle with $a = 50$ nm. Here, we investigate small particles with $a = 50$ nm. Figure 8 shows the influence of salt concentration $n_0$ on the evolution of concentration. One can see that the concentration, with the decrease of $n_0$, increases slowly at the drying end, keeping the uniform distribution along the H-S cell over time. As a

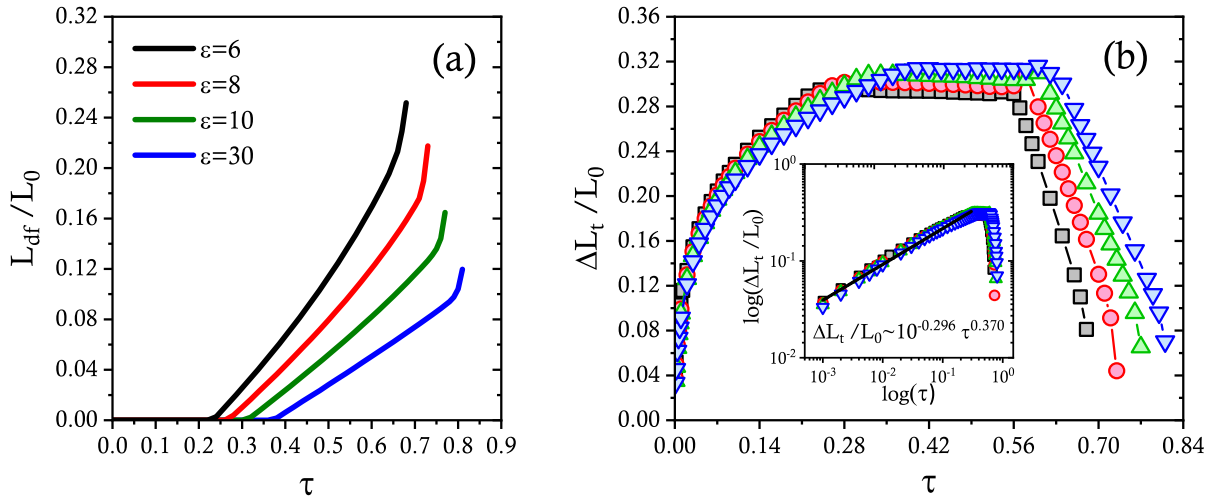


FIG. 7. (a) The evolution of the drying front and (b) the evolution of the liquid-solid transition layer for different confinement parameters. The inset in (b) shows the log-log plot of the liquid-solid transition layer over time. The growth of the liquid-solid transition font $L_{tf}$ before the formation of the drying front can hold the same linear behavior. Other parameters are the same in Fig. 5.

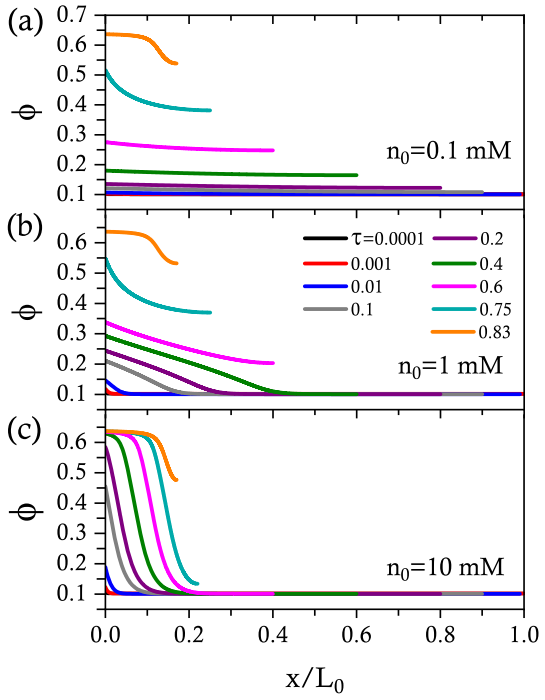


FIG. 8. Time evolution of concentration of the charged particles ($a = 50$ nm, $\gamma = 0.132\,\mathrm{e\,nm^{-2}}$) for various monovalent salt loadings. Here, $\varepsilon = 200$ is used to keep the same cell height for the large particles ($a = 100$ nm). Other parameters are Pe $= 50$ and $\phi_0 = 0.1$.

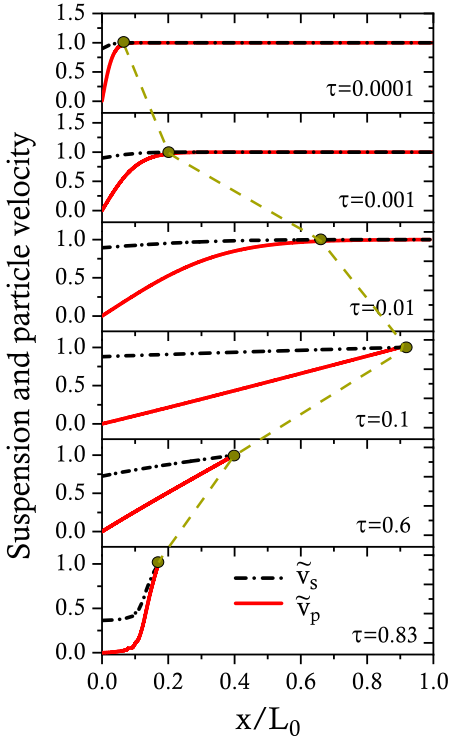


FIG. 9. The evolution of the particles velocity and the suspension velocity when drying the suspension with low salt concentration $n_0 = 0.1$ mM. The yellow dashed line connects the liquid-solid transition front $L_{tf}$ over time. Other parameters are the same in Fig. 8.

consequence, the dense packing zone is seen only at the later stage of the drying.

The occurrence of such a phenomenon is most likely caused by the aggregation formed by the charged particles with notably high collective diffusivity due to low salt loadings. The formed aggregates constitute a colloidal framework as a bulk in the suspension, which, in turn, hinders particle transport along the cell. That would explain the difficulty in increasing the concentration profile at the drying end. The entire profile along the H-S cell exhibits the trend of uniform distribution. We characterize the velocity profiles of the particles and the suspension for the low salt loading, $n_0 = 0.1$ mM, in Fig. 9. As seen in Fig. 9, the LST front in which the particles and the suspension are divergent in velocity recedes inside the H-S cell to meet the liquid-air interface in an extremely short time ($\tau < 0.01$). That is to say, the initial suspension at the pure liquid state has rapidly turned into the liquid-solid transition state. In this state, the LST rapidly formed at the initial drying. The clusters of charged particles are compacted in a colloidal network that appears to reside in the dispersion, which is characterized as a yield stress material or gel-like material instead of a simple fluid. This colloidal network prevents the individual particle from leaving freely. Our treatments corroborate the experimental observations from Goehring *et al.* [28]. On the other hand, the lower the salt loadings, the longer the Debye length of electric field, which indicates that the interattraction is occupied among charged particles, and as a consequence, the aggregates are formed easily. With the increasing salt concentration, the charged particles are well dispersed, since the Debye length becomes shorter and the repulsion effect dominates particle interactions. According to these analyses, we conclude that charged particles prefer to aggregate in the suspension with significantly large collective diffusivity, which eventually leads to a colloidal gel-like network in the suspension.

Here, we study further the evolution of the drying front and the liquid-solid transition layer for different salt concentrations in Fig. 10. As expected, in Fig. 10(a), the drying front appears at later time of the drying for low salt loadings, and it is seen to recede rapidly inside the cell. Figure 10(b) shows that, for the low salt concentration, the initially formed LST front recedes immediately to meet the liquid-air interface far from the drying side, which signifies that the LST front has disappeared very quickly, and only the liquid-air interface is forced to shrink towards the drying end. We also find that the different salt loadings can hardly alter the linear growth behavior of the LST front, as seen in double-log plot in Fig. 10(b).

At last, we examine our theoretical model with the experiments by Goehring *et al.*, in which the suspensions of the charged silica spheres were directionally dried in the H-S cell. The information provided by Goehring *et al.* is too limited to determine some necessary parameters for calculations within the model. In addition, the coordinate scale they used for representing the measurements differs from that we used in the model. But the comparisons are still accessible if we follow a simple route. We invoke the length they processed as the length $L_0$ in our model. As a result, the concentration profile could be calculated, in principle, at a time close to the initial state. (The time for the concentration data recorded by

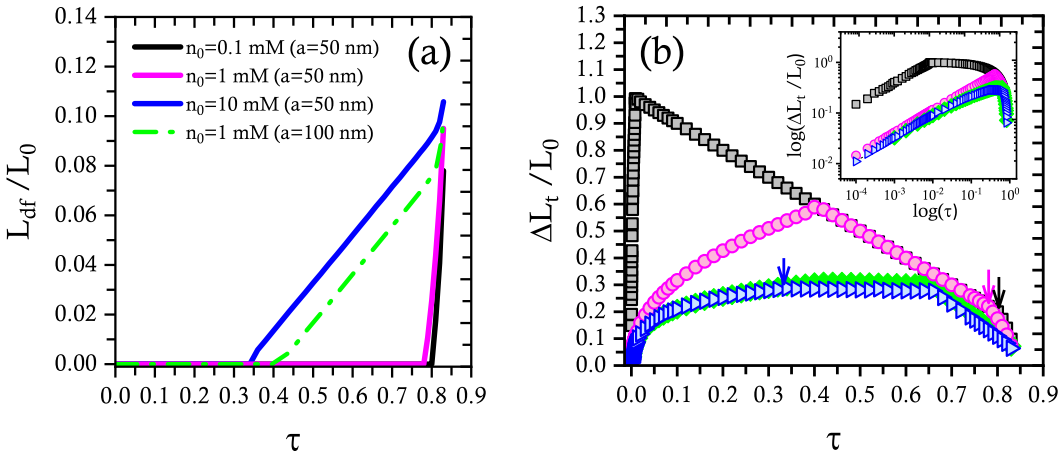


FIG. 10. (a) The evolution of drying front and (b) the evolution of liquid-solid transition layer for different salt loadings. The inset is the log-log plot of the main profiles in (b). The time guided by the arrow in (b) is for the occurrence of the drying front. Other parameters are the same as those in Fig. 8.

Goehring *et al.* was not given). Such a simple transformation route is feasible in two ways: (i) we can naturally treat the drying rate measured by Goehring *et al.* as the velocity of evaporated water $v_f$ in our model, and (ii) we avoid an extremely large Peclet number in the model. All the useful data, such as the length, particle diffusivity and radius, average evaporation rate, and salt concentration can be explicitly cited in the supplementary material (see Ref. [28]). Utilizing these source data, we are able to roughly estimate the drying Peclet number in the model.

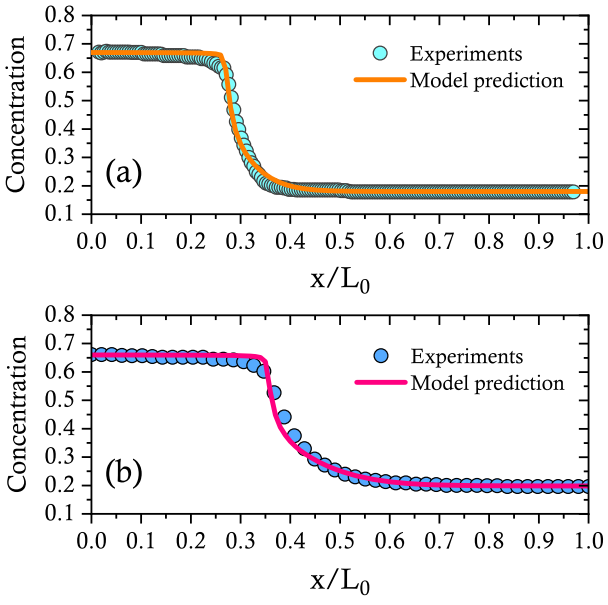


FIG. 11. Reproducing the experiments by the theoretical model. (a) The experiments for colloidal silica spheres with $a = 14$ nm, $\gamma = 0.5\,\mathrm{e\,nm^{-2}}$, and the salt concentration $n_0 = 0.5$ mM. The diffusion constant of an individual particle is given by $D_0 = 15.3\,\mu\mathrm{m}^2/\mathrm{s}$ and the average evaporation is $v_f = 0.41\,\mu\mathrm{m/s}$. The parameters used for calculation by our model are estimated roughly as $\mathrm{Pe} = 320$, $\tau = 0.15$, and $\phi_0 = 0.193$. (b) The experiments for colloidal silica spheres with $a = 8$ nm, $\gamma = 0.5\,\mathrm{e\,nm^{-2}}$, and salt concentration $n_0 = 5$ mM. The diffusion constant of an individual particle is given by $D_0 = 26.8\,\mu\mathrm{m}^2/\mathrm{s}$ and the average evaporation is $v_f = 0.28\,\mu\mathrm{m/s}$. The parameters used for calculation by model are estimated roughly as $\mathrm{Pe} = 105$, $\tau = 0.19$, and $\phi_0 = 0.195$.

To a certain degree, a good agreement can be seen in comparisons between the experiments and the predictions as illustrated in Fig. 11. In the present work, only rough theoretical calculations using the experimental conditions can be made. The close correlation between the theory and certain experiments, however, is not the goal of the present study. We would like to propose a landscape in which the simple model we present is vigorous enough to characterize transport dynamics in directional drying of the suspensions consisting of charged particles dispersed in a confined microchannel. A further research topic will be the exploration of whether the present theoretical framework can be extended to the drying dynamics of nonspherical charged particles, such as rods and platelets, with similar conditions to those in the present problem.

## IV. CONCLUSIONS

We have theoretically reported the transport dynamics of charged colloidal particles in directional drying of suspensions in a confined microchannel. A nonequilibrium advection-diffusion model with 1D configuration is developed by explicitly considering both the electrostatic interaction among the charged particles and the viscous flow confined to a H-S channel. It is found that the evolution of drying is affected by the resultants of multiple parameters, including average evaporation rate, confinement ratio, monovalent salt concentration, and properties of the charged colloidal particles. By numerical calculations, we show that the drying front appears after the liquid-solid transition front, and they recede together into the H-S cell in different dynamic behaviors, namely, the drying front and transition front evolve over time with the linear law and the power law, respectively. The higher evaporation rate leads to the more rapid formation of the drying front but creates a thinner liquid-solid transition layer.

The confinement effect is shown to facilitate evaporation of the solvent, but to slow down the particle transport in the

Hele-Shaw cell, which directly leads to a longer fully dried film, but with a shorter drying time for this film. Under confinement, the drying front exhibits nonlinear growth behavior, but the liquid-solid transition front can evolve while still holding the linear law in log-log plots. We also find that the decreasing concentration of monovalent salt can result in the significantly large collective diffusivity of charged particles, and these particles in such a state prefer to aggregate to form a colloidal network in the suspension.

As the colloidal particles aggregate due to low salt loadings, the liquid-solid transition state is found to form immediately, and the suspension in such state behaves as a yield-stress or gel-like material instead of as a simple fluid. Consequently, particle transport is hindered, as well as the formation of the drying front at the drying end. These drying behaviors alter dramatically with different salt loadings. The present theoretical results are also shown to be consistent with the recent experiments. The current insight is expected to shed light on the exploration of the drying dynamics behavior of anisometric charged colloidal particles.

## ACKNOWLEDGMENTS

We thank Jan Gerston for useful comments on the manuscript. This work was supported by Grant No. 21434001 of the National Natural Science Foundation of China (NSFC).

[1] W. B. Russel, AICHE J. **57**, 1378 (2011).
[2] A. F. Routh, Rep. Prog. Phys. **76**, 046603 (2013).
[3] R. D. Deegan, O. Bakajin, T. F. Dupont, G. Huber, S. R. Nagel, and T. A. Witten, Nature (London) **389**, 827 (1997).
[4] R. D. Deegan, O. Bakajin, T. F. Dupont, G. Huber, S. R. Nagel, and T. A. Witten, Phys. Rev. E **62**, 756 (2000).
[5] U. Thiele, Adv. Colloid Interface Sci. **206**, 399 (2014).
[6] L. Daubersies and J.-B. Salmon, Phys. Rev. E **84**, 031406 (2011).
[7] F. Giorgiutti-Dauphine and L. Pauchardb, Eur. Phys. J. E **41**, 32 (2018).
[8] J. Leng, Phys. Rev. E **82**, 021405 (2010).
[9] P. Lidon and J. B. Salmon, Soft Matter **10**, 4151 (2014).
[10] S. Inasawa, Y. Oshimia, and H. Kamiya, Soft Matter **12**, 6851 (2016).
[11] K. Abe and S. Inasawa, Phys. Chem. Chem. Phys. **20**, 8935 (2018).
[12] C. Allain and L. Limat, Phys. Rev. Lett. **74**, 2981 (1995).
[13] E. R. Dufresne, E. I. Corwin, N. A. Greenblatt, J. Ashmore, D. Y. Wang, A. D. Dinsmore, J. X. Cheng, X. S. Xie, J. W. Hutchinson, and D. A. Weitz, Phys. Rev. Lett. **91**, 224501 (2003).
[14] E. R. Dufresne, D. J. Stark, N. A. Greenblatt, J. X. Cheng, J. W. Hutchinson, L. Mahadevan, and D. A. Weitz, Langmuir **22**, 7144 (2006).
[15] L. Goehring, W. J. Clegg, and A. F. Routh, Langmuir **26**, 9269 (2010).
[16] L. Goehring, W. J. Clegg, and A. F. Routh, Phys. Rev. Lett. **110**, 024301 (2013).
[17] N. Birk-Braun, K. Yunus, E. J. Rees, W. Schabel, and A. F. Routh, Phys. Rev. E **95**, 022610 (2017).
[18] M. Nassar, A. Gromer, D. Favier, F. Thalmann, P. Hebraudb, and Y. Holl, Soft Matter **13**, 9162 (2017).
[19] B. Yang, J. S. Sharp, and M. I. Smith, ACS Nano **9**, 4077 (2015).
[20] P. C. Kiatkirakajorn and L. Goehring, Phys. Rev. Lett. **115**, 088302 (2015).
[21] A. G. Marin, H. Gelderblom, D. Lohse, and J. H. Snoeijer, Phys. Rev. Lett. **107**, 085502 (2011).
[22] F. Boulogne, L. Pauchard, and F. G. Dauphine, R. Botet *et al.*, Eur. Phys. Lett. **105**, 38005 (2014).
[23] C. Noirjean, M. Marcellini, and S. Deville, Phys. Rev. Mater. **1**, 065601 (2017).
[24] H. Y. Erbil, Adv. Colloid Interface Sci. **222**, 275 (2015).
[25] A. F. Routh and W. B. Russel, AICHE J. **44**, 2088 (1998).
[26] A. Sarkar and M. S. Tirumkudulu, Langmuir **25**, 4945 (2009).
[27] C. Loussert, A. Bouchaudy, and J.-B. Salmon, Phys. Rev. Fluids **1**, 084201 (2016).
[28] L. Goehring, J. Li, and P. C. Kiatkirakajorn, Philos. Trans. R. Soc. A **375**, 20160161 (2017).
[29] E. Trizac, L. Bocquet, M. Audouy, and H. H. von Grunberg, Langmuir **19**, 4027 (2003).
[30] L. Belloni, Colloids Surf. A **140**, 227 (1998).
[31] R. Roa, D. Menne, J. Riest, P. Buzatu, E. K. Zholkovskiy, J. K. G. Dhont, M. Wessling, and G. Nägele, Soft Matter **12**, 4638 (2016).
[32] G. N. Choi and I. M. Krieger, J. Colloid Interface Sci. **113**, 101 (1986).
[33] S. S. L. Peppin, J. A. W. Elliott, and M. G. Worster, J. Fluid Mech. **554**, 147 (2006).
[34] W. B. Russel, D. A. Saville, and W. R. Schowalter, *Colloidal Dispersions* (Cambridge University Press, Cambridge, 1989).
[35] Z. D. Cheng, J. X. Zhu, P. M. Chaikin, S.-E. Phan, and W. B. Russel, Phys. Rev. E **65**, 041405 (2002).
[36] S. Heitkam, Y. Yoshitake, F. Toquet, D. Langevin, and A. Salonen, Phys. Rev. Lett. **110**, 178302 (2013).